DRAG FORCE MEASUREMENTS OF VEGETATION ELEMENTS

T. Schoneboom[1], J. Aberle[2], C.A.M.E. Wilson[3], and A. Dittrich[4]

[1] Leichtweiß-Institute for Hydraulic Engineering, Technische Universität Braunschweig, Beethovenstr. 51a, 38106 Braunschweig, Germany; e-mail: t.schoneboom@tu-bs.de

[2] Leichtweiß-Institute for Hydraulic Engineering, Technische Universität Braunschweig, Beethovenstr. 51a, 38106 Braunschweig, Germany; e-mail: j.aberle@tu-bs.de

[3] Hydroenvironmental Research Centre, Cardiff School of Engineering Queen's Buildings, Newport Road, Cardiff, CF24 3AA, UK; e-mail: wilsonca@Cardiff.ac.uk

[4] Leichtweiß-Institute for Hydraulic Engineering, Technische Universität Braunschweig, Beethovenstr. 51a, 38106 Braunschweig, Germany; e-mail: a.dittrich@tu-bs.de

ABSTRACT

This paper investigates hydrodynamic drag forces caused by different types of single vegetation elements using a novel drag force measurement system. The design and calibration of the drag force measurement system, which is based on strain gauges, is described. Using rigid cylinders, artificial, and natural flexible vegetation elements, the applicability of the system is shown. A new parameter for data interpretation, the lever arm L, is introduced and the measured drag forces are discussed with respect to plant morphology and further biological properties. Special attention is given to the effect of streamlining of the plants under flow action.

Keywords: drag force, natural vegetation, artificial vegetation, rigid cylinders, streamlining

1 INTRODUCTION

Flooding is the most common natural disaster worldwide and the third pan-European state of the environment report prepared by the European Environment Agency (EEA 2003) points out that the risk of catastrophic flood events is expected to increase as a consequence of climate change. Recent flood events showed that current environmental and technical river management strategies, such as providing additional retention areas and rising of embankments are not adequate to mitigate the effects of floods. As a further challenge, the EU Water Framework Directive (WFD) requires the achievement of a good ecological status of rivers by 2015, which is in contrast to another flood protection measure: floodplain vegetation clearing. Thus, it is indispensable to develop sustainable strategies which are in accordance with both flood management and ecology. The key to developing such strategies is the identification and assessment of physical processes, which dominate the complex interaction between water flow and vegetation, since vegetation increases flow resistance and changes backwater profiles (Yen 2002). Although significant advances have been made recently, the effects of vegetation on the flow and vice versa are still not fully understood.

An abundance of investigations have been carried out in which vegetation has been simulated using rigid cylindrical elements and for such boundary conditions, the flow properties are widely understood (e.g., Lindner 1982). In contrast to rigid elements, the physical processes governing the drag forces exerted by flexible vegetation are not yet fully understood as they depend on many hydraulic and biomechanical properties. In order to

investigate flow resistance induced by flexible vegetation, several devices have been constructed to measure drag forces directly (e.g., Armanini et al. 2005, Wilson et al. 2005, Statzner et al. 2006, Callaghan et al. 2007). Such direct measurements of drag forces have considerable advantages, e.g., quantification of drag fluctuations due to dynamic response of the elements. Furthermore, using drag force devices it becomes possible to investigate the influence of biomechanical properties, e.g. bending stiffness, leaf biomass, leaf area, shape, etc. on drag forces. Such measurements are required to enhance our understanding of the relevant physical processes. Moreover, in conventional experiments drag induced by vegetation is often represented by bulk energy loss coefficients (e.g. Manning-Strickler's n, or Darcy-Weisbach friction factor f). Bulk approaches are appropriate only for one-dimensional considerations and a detailed investigation of the influence of the vegetation on the velocity field within the water depth or the river width is not possible following this methodology (Wilson et al. 2005). For this purpose, it is necessary to represent the normal stresses induced by bed roughness and vegetation separately. Such approaches can be developed measuring drag forces exerted by single elements and/or in a canopy.

The scope of this paper is presenting the design and preliminary results of a novel submersible drag force measurement system (DFS). The design of the DFS is based on the system developed and used by Wilson et al. (2005). Special attention was given to a high temporal resolution and accuracy as well as to a cost-efficient production enabling simultaneous measurements using several devices. The performance of the DFS is demonstrated on the basis of drag force measurements using natural and artificial vegetation elements.

2 DRAG FORCE MEASUREMENT DEVICE

The drag force measurement system (DFS) presented in this paper is an enhancement of the system described by Wilson et al. (2005, 2008). The design of the DFS is based on the employment of a series of strain gauges enabling the measurement of drag forces with high accuracy and temporal resolution. The device, shown in Figure 1, consists of a 140 mm long, 20 mm wide, and 3 mm thick stainless steel beam (X5 CO-NI 18-10 steel) being connected to a base plate by a rigid joint. A free movable aluminium base plate is fixed to the top of the steel beam in which vegetation elements can easily be fixed using the screw thread inside the head plate.

Drag forces are measured using eight active Tokyo Sokki Kenkyujo Co. Ltd. strain gauges (Type FLA-3-350-C4-17) which are mounted to the centreline of the stainless steel beam. The strain gauges are configured as two Wheatstone full bridge configurations being separated by distance l (Pos. 1 and 2 in Figure 1). Wheatstone full bridges are formed by four gauges and have the advantage that normal strain (in the beam) and temperature induced strain are compensated (Hoffmann, 1987). A further advantage of Wheatstone full bridges is that interfering factors such as bridge internal connections are suppressed, resulting in a temperature insensitive setup. In order to protect the DFS from humidity, a plastic tube is connected to the head plate preventing water ingress into the plastic tube (Figure 1).The strain gauges are connected to an amplifier (National Instruments series NI DAQmx 9237) and the corresponding signal is logged by a PC.

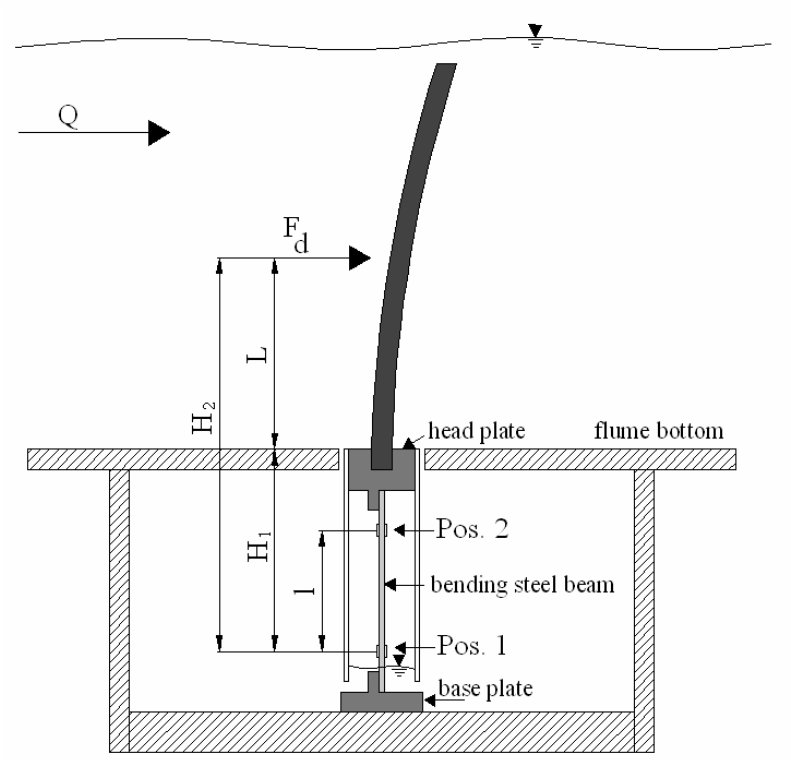

Figure 1 Drag force measurement system (DFS) consisting of two Wheatstone full bridges mounted at Positions 1 and 2 being separated by distance *l*.

When subjected to flow, the vegetation element acts as a cantilever in bending. This cantilever is attached to a steel beam embedded in the DFS which deforms generating bending moments and compression strains ε_1 and ε_2 at positions 1 and 2. These are measured directly by the strain gauges. For the calculation of the bending moments it is necessary to relate strain to normal stress on the bending beam surface which is achieved using the relationship $\sigma = 0.25\varepsilon E$ for a Wheatstone full bridge (Keil, 1995) where E = elastic modulus of the steel beam. Knowing σ, the bending moments can be calculated as follows (Keil, 1995):

$$M = \sigma W \tag{1}$$

where the section modulus $W = wt^2/6$, with w = width and t = thickness of the steel beam, respectively. The use of two Wheatstone bridges enables the determination of the lever arm H_2 through:

$$H_2 = l\left(\frac{M_1}{M_1 - M_2}\right) \tag{2}$$

Knowing both moments M_1 and M_2, the resulting force F_D acting onto the vegetation element can be calculated as follows:

$$F_D = \frac{M_1 - M_2}{l} \tag{3}$$

With the given distance H_1 of the lower Wheatstone full bridge to the top of the head plate, the lever arm of the acting force with respect to the flume bottom is $L = H_2 - H_1$.

2.1 Calibration

Equations (1) - (3) show that the knowledge of steel properties as well as the geometrical measures H_1 and l is necessary for the determination of the drag force. Each load yields strain values which are transformed into the corresponding bending moment by assuming a given value of the modulus of elasticity (E = 200 N/mm²). However, the precision of the beam's manufacture is crucial as manufacturing imperfections of only Δt = 0.01 mm in beam thickness t would result in an error of approximately 0.67 %. The resulting drag force would be affected in a linear fashion. Thus, to account for bending steel beam inaccuracies a correction factor k must be introduced. This factor can be estimated by applying known forces at given distances L and plotting the corresponding moments at position 1 and 2 against each other. For perfect conditions, the gradient of the corresponding straight line should be equal to unity. If the gradient is not equal to unity, the bending moment at position 2 should be corrected using the gradient k of the M_1-M_2 straight line according to:

$$M_2 = \sigma_2 \cdot W_2 / k \tag{4}$$

A further parameter requiring attention is the distance l between the Wheatstone full bridges. Due to the setup of the bridges with four active gauges a direct and accurate measurement of l is complicated. However, using measurements with known loads at known distances (i.e., knowing M_1 and M_2), l can be calculated using equation (3). The correction factor k and the distance between the Wheatstone bridges have been estimated from a set of special calibration measurements in which the DFS was placed into a horizontal position (i.e., rotated by 90°). A rigid cylinder was then inserted into the head plate and loaded with known weights (50, 100, 200 g) at various known distances L (L = 0, 2, 4, 6, 8, 10, 12, 14, 16 and 18 cm, respectively). The analysis of these calibration measurements resulted in a correction factor k = 1.0086 and a mean distance of the Wheatstone bridges of l = 68.24 mm. Moreover, using the measurements with L = 0, the distance of position 2 to the top of the head plate was estimated to H_1 = 0.148 m.

Following the calibration, the performance of the DFS was evaluated by a series of measurements in which the rigid cylinder attached to the horizontally aligned DFS was loaded with known forces (1, 2, 5, 10, 20, 50, 100, 200, 500g) at given distances L = 0, 10, 18 cm. The corresponding results are shown in Figure 2. Figure 2A shows an almost perfect correlation between input and output force independent of the lever arm; the maximum error in the drag force is 0.02 N (Figure 2B). Furthermore, Figures 2C and 2D show that increasing load does neither increase the standard error nor the standard deviation of measured forces.

Further calculations based on the assumption of a linear elastic stress-strain curve indicate that the limit of elasticity in bending is reached at a force of 15 N at a lever arm L = 20 cm (or a critical moment of M = 5.7 Nm). The estimation of the elastic aftereffect of the steel beam was investigated in a long-term test. For this purpose, a total load of 1.021 N was attached to the mounted cylinder at an arbitrary distance for four hours resulting in a maximum deviation from the input force of +0.038 N within this time period. After unloading, the DFS shows only a negligible drift of +0.0023 N. Initial analyses of time series of dynamically induced forces showed the ability of the system to identify dynamic fluctuations precisely due to the high sampling rate.

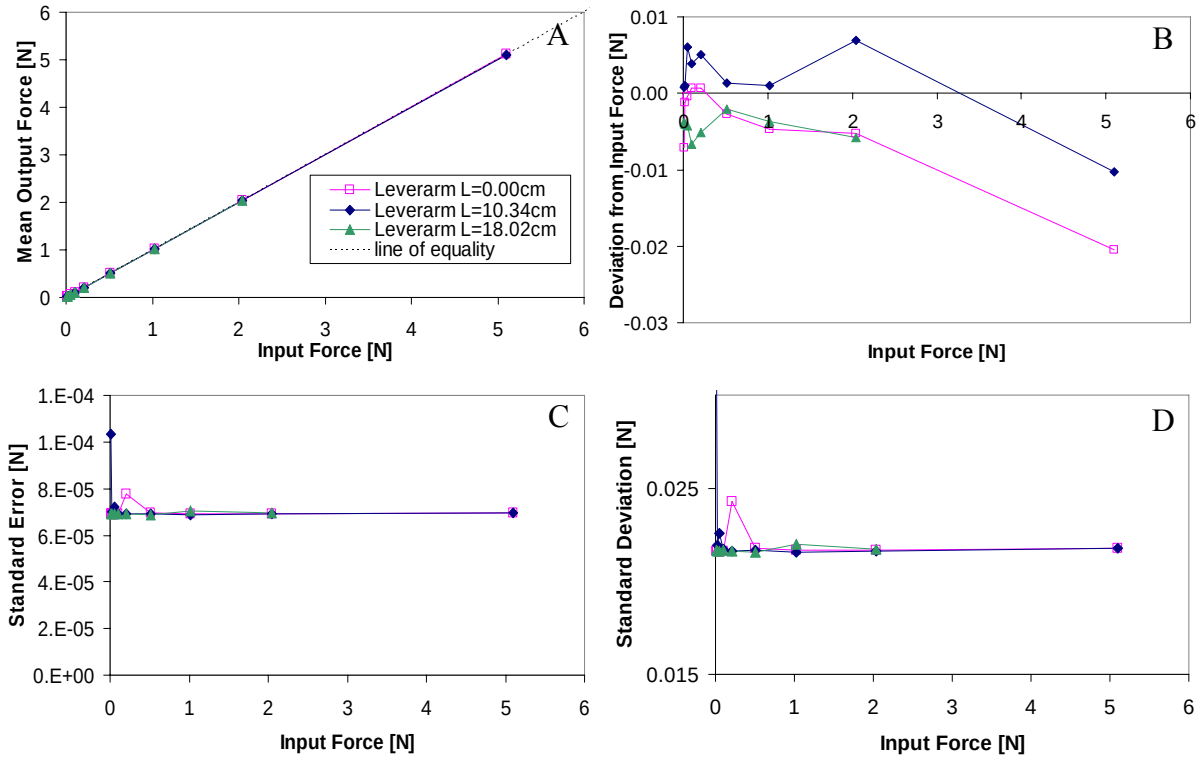

Figure 2 Results of the calibration of the DFS including effect of variation of lever arm L. (A) Relationship between input force and mean output force F_d. (B) Deviation from input force to mean output force. (C) Standard error $s(\bar{x})$ and (D) standard deviation s(x) of mean output force for a given input force.

3 EXPERIMENTAL METHODOLOGY

Experiments were carried out in a 20 m long race-track shaped flow channel with a pipe diameter of 19 cm in the laboratory of the Leichtweiß-Institute (Figure 3 A). The flow velocity (*u)* in the channel was controlled by a calibrated speed-controlled propeller. A container made of plexiglass (dimensions 0.6 m x 0.5 m) was used to house the DFS. This was located in the working section of the pipe and at a distance of 16 m from the propeller. The DFS and the attached vegetation element were orientated in an upside-down position (Figure 3 B).

Three different types of natural and artificial vegetation, shown in Figure 4, were selected for these preliminary experiments: 1) natural, flexible poplar (*Populus nigra*) and willow (*Salix alba*) branches; 2) flexible plastic poplar and willow branches and artificial sedges (*Carex sp.*); and 3) a rigid steel and plastic cylinder with a diameter of 1.0 cm, respectively. Details of the plant characteristics are given in Table 1. The living willow and poplar branches were collected in the field and taken directly to the laboratory for testing. Please note that we identified the frontal projected area A_p as the area of the plant under no flow action and corresponding to the elevations shown in Figure 4. Due to the special shape of the artificial willow, the leaf area is lower than the frontal projected area. Drag force measurements for these vegetation elements were carried out at a sampling rate of 1613 Hz, for a sampling period of 60 s and for 12 different flow velocities ranging from 0.27 m/s to 2.27 m/s.

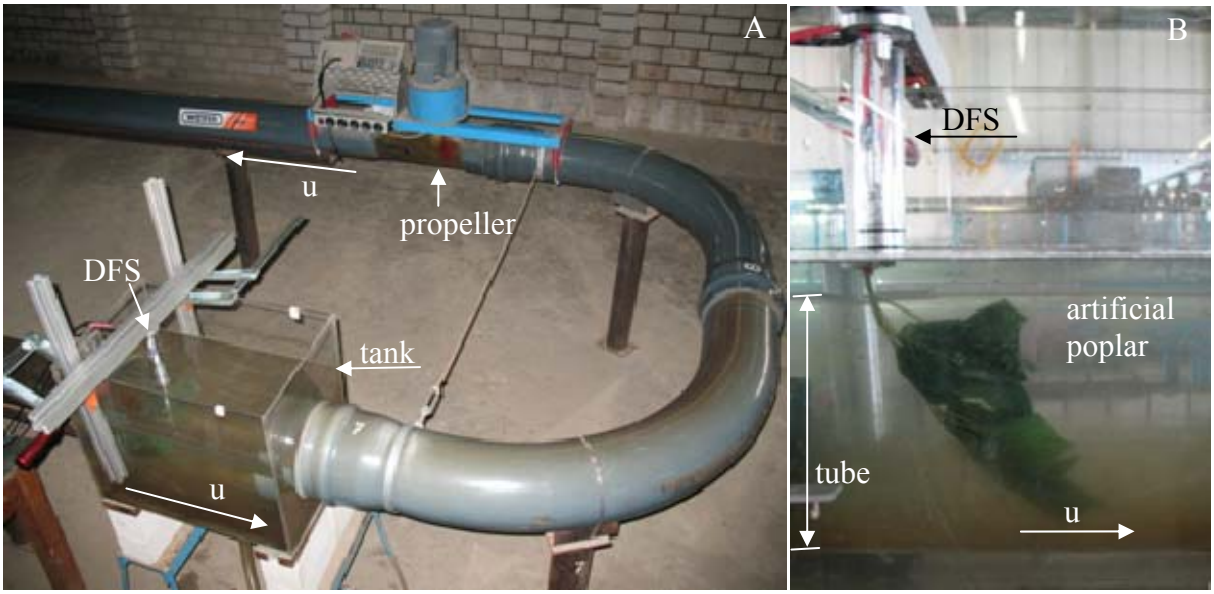

Figure 3 Flow channel

Table 1 Vegetation characteristics. LAI is the leaf area index; leaf area is defined by the area when leafs are flatten and scanned; A_p is the area of the plant under no flow action

	Natural		Artificial			Cylinder	
	Willow	Poplar	Willow	Poplar	Sedge	Plastic	Steel
height [cm]	37	24	37	23	20	19	19
leaf number	137	45	35	12	14	n.a.	n.a.
leaf area [cm^2]	572	520	447	361	269	n.a.	n.a.
LAI	0.95	2.27	1.11	1.11	1.37	n.a.	n.a.
A_p [cm^2]	533	312	516	200	116	n.a.	n.a.

Figure 4 Side elevation of the investigated vegetation elements (from left to right: natural willow; artificial willow; natural poplar; artificial poplar; artificial sedge; plastic cylinder; and steel cylinder; each colour mark on the scale is 10 cm)

4 RESULTS & DISCUSSION

The time-averaged drag forces for the seven test elements are shown as a function of bulk flow velocity (*u)* in Figure 5. The figure shows distinct differences between the rigid (cylinders) and flexible (artificial and natural) vegetation types. The measurements with the rigid cylindrical elements show an almost linear relationship between drag force and the squared of the velocity. It is interesting to note that, although both cylinders had an identical geometry, significantly different forces were measured at higher velocities. This result can be explained by the strong vibrating behaviour of the plastic cylinder at higher velocities in contrast to the steel cylinder. The magnitude of the flow induced vibrations becomes apparent in Figure 5B whereby the time-averaged drag force curves are presented together with the corresponding standard deviation for the time series. The standard deviation for the plastic cylinder measurements is a minimum value of 0.08 N at a velocity of 0.77 m/s. While for higher velocities, the standard deviation increases continually to reach a maximum value of 12 N at the maximum velocity examined. Note that the standard deviation for this case is even larger than the mean value, implying that extremely strong vibrations were predominant.

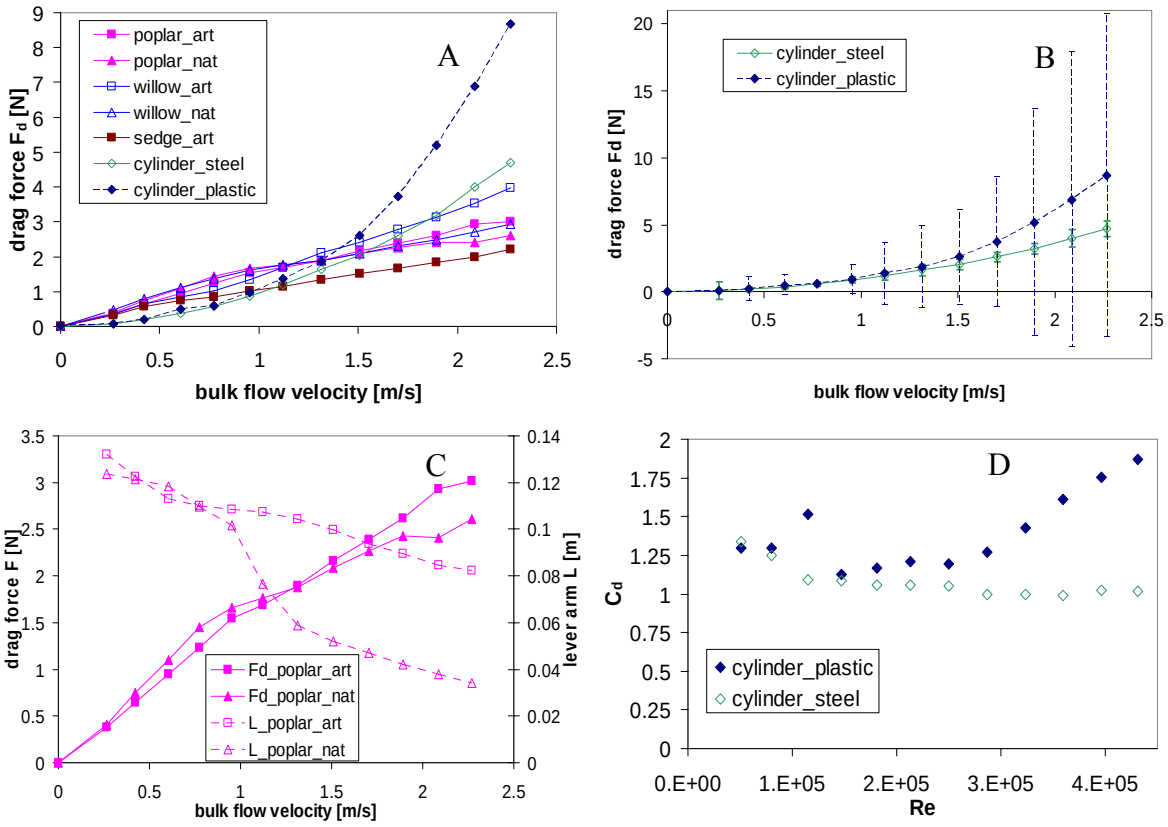

Figure 5 Results of the drag force measurements of vegetation elements. (A) Force-velocity relationship for all elements. (B) Force-velocity relationship and standard deviation for steel and plastic cylinder. (C) Force-velocity and lever arm-velocity relationship for natural (nat) and artificial (art) poplar. (D) C_d-*Re* relationship for plastic and steel cylinder.

In contrast to the plastic cylinder, the drag force standard deviation measured for the steel cylinder reached a maximum value (0.68 N) at the relatively lower velocity (0.27 m/s) i.e. the standard deviation for the steel cylinder is less than an order of magnitude smaller than the plastic cylinder, indicating the significance of material properties on dynamics of drag

forces. Figure 5D shows the drag coefficient C_D as a function of Reynolds number for both cylinders. The drag coefficients have been calculated using the standard drag force formula $F_D = 0.5\rho C_D A_F u^2$ where ρ = fluid density and A_F = frontal area (Hoerner, 1965). For the steel cylinders, the evaluated drag coefficients were in the range of 1.0 to 1.1 for Reynolds numbers $Re \approx 1.1\text{x}10^5$, this is in keeping with previous research studies (Sumer & Fredsøe, 1997). Due to vibration effects, it is not possible to discuss drag coefficients of the plastic cylinder unambiguously.

In contrast to the drag forces exerted by the rigid elements, the experiments with the flexible plants show an almost linear relation between drag force and velocity. Similar results have been reported by Vischer & Oplatka (1998), Freeman et al. (2000), Armanini et al. (2005), Wilson et al. (2005, 2008) and Statzner et al. (2006). The deviation from the velocity-squared relationship has been associated with streamlining effects in these studies. In fact, Freeman (2000) showed that leaf shape changed with velocity and, as a consequence of streamlining, that drag coefficient and resistance coefficient decreased with velocity. These findings are also in agreement with Vogel (1994), who reported that the major contributor to the drag of most trees is the drag of the leaves and that reshaping of the leaves (i.e., the change of the frontal area) is a critical process in generating drag.

Figure 5C shows the force-velocity relationship in combination with the lever arm-velocity relationship for the experiments carried out with the natural and artificial poplar. The figure shows that the lever arm (L) is, for both elements, almost identical up to a velocity of 1 m/s. For a velocity of 1.12 m/s, the lever arm of the natural poplar suddenly decreases. We associate this decrease with an exceedance of the maximum load on the stem, i.e. the flexural rigidity of the natural poplar stem changed significantly at this load. Note that in general, streamlining and bending effects result in a decreasing lever arm L. As both investigated elements have approximately the same height we conclude that up to a velocity of 1.12 m/s the flexural rigidity of the artificial poplar is similar to its 'natural' counterpart. The force-velocity relationship is linear for both poplars and we associate the slight differences with differences in leaf area (see Table 1). However, a final evaluation of the ability of the artificial poplar to represent a natural one will only be possible following further tests in which parameters such as leaf area index (LAI) and further properties (e.g., number of leaves, stem diameter etc.) should be identical for the natural and artificial plants.

Compared to the poplar, larger differences were observed for the relationship between lever arm and velocity for the artificial and natural willow elements (Figure 6). We associate these differences with the diversity of the natural and artificial plant morphology and material properties. For example, the natural willow is characterized by two branches with a high leaf area close to the bearing point (Figure 4). Thus, this morphology will, compared to its artificial counterpart, result in a lower lever arm due to load transmission close to the head plate (see Figure 6).

Although differences in the relationship between velocity and lever arm can be observed, the drag forces are reasonably similar for identical velocities. The differences in the velocity-lever arm relationship suggest that the streamlining is different for the plant elements. This behaviour is to be expected since although the frontal area A_p of the artificial and natural willow elements were similar, there are differences in the plant characteristics notably the leaf number and shape. This aspect will be investigated in more detail in our future studies.

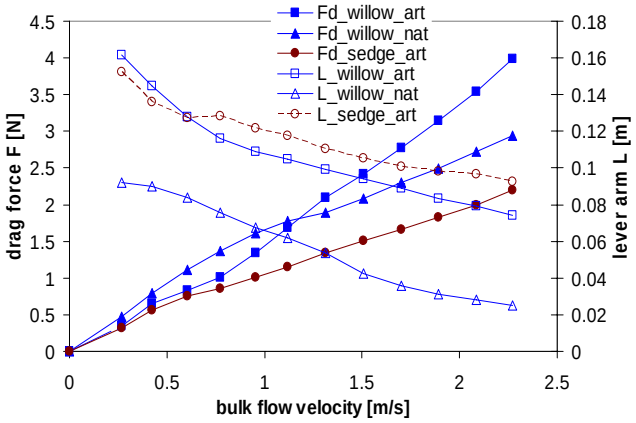

Figure 6 Force-velocity relationship for natural and artificial willow and artificial sedge.

The force-velocity relationship of the artificial sedge is characterised by a linear relationship for flow velocities greater than 0.7 m/s. In general, lower drag forces were observed for this plant type which was expected due to plant morphology (see Table 1). Note that the artificial sedge was used in the flow resistance experiments of Järvelä (2006). Based on canopy experiments he found that the sedges behaved quite differently than natural vegetation. The initial analysis of drag forces exerted by the sedges presented in this paper show that, the lever arm as well as the force-velocity relationship change quite significantly for velocities greater than 0.6 m/s. However, as the canopy experiments of Järvelä (2006) were carried out only for flow velocities less than 0.6 m/s this observation may not be used as an explanation of the results of Järvelä (2006). Therefore, further investigations are required taking into account streamlining effects and dynamic plant behaviour not only for single plant elements but also for groups of elements (canopies). For this purpose it is planned to construct several DFS-sensors and to use them simultaneously at various positions within the canopy. Additional information on frontal projected plant area will be obtained using a submersible digital camera. Such data will enable further insight into the complex interaction between flow and vegetation.

5 SUMMARY & CONCLUSIONS

This paper introduces the design and calibration of a novel drag force measurement system which was used to measure drag forces exerted by natural and artificial vegetation and rigid cylinders. The device, based on strain gauges, can be used to measure drag forces with a high accuracy (0.01 N) and temporal resolution (1613 Hz). The strain gauges are designed to form two Wheatstone full bridges, so that the sensor is not affected by normal strain in the steel beam, temperature induced-strains, and the internal connections of the bridges.

The study revealed that large differences in drag force magnitudes can be observed for two geometrical identical rigid cylinders manufactured of different materials. These differences could be explained by flow-induced vibrations, which were significant for the plastic cylinder. For the steel cylinder, drag coefficients were observed for large Reynolds numbers which were in keeping with previous studies. The system was also used to measure drag forces exerted by different natural and artificial plants. These measurements showed that the device may be used to identify artificial plants which can be used to model natural vegetation, i.e. which show the same dynamic behaviour as natural plants. For this purpose,

the parameter lever arm (*L)* has been proposed for data interpretation, which can be used to gain information on plant morphology, flexibility and streamlining. Further experiments will be carried out to investigate the suitability of lever arm to parameterise flexibility and streamlining and to further study the hydrodynamic behaviour of natural and artificial vegetation elements by analysing the time series of drag forces.

ACKNOWLEDGMENTS

The research was conducted under contract AB 137/3-1 from DFG (Deutsche Forschungsgemeinschaft). The authors are grateful to U. Ecklebe for technical support.

REFERENCES

Armanini, A., Righetti, M., Grisenti, P. (2005). "Direct measurement of vegetation resistance in prototype scale." *J. Hydraul. Res.* 43(5), 481–487.

Callaghan, F. M., Cooper, G. G., Nikora, V. I., Lamoroux, N., Statzner, B., Sagnes, P., Radford, J., Malet, E., Biggs, B. J. F. (2006). "A submersible device for measuring drag forces on aquatic plants and other organisms." *New Zeal. J. Mar. Freshwat. Res.* 41(1), 119-127.

EEA (2003). "Europe's environment: the third assessment." Environmental Assessment Report No. 10, European Environment Agency, Copenhagen.

Freeman, G., Rahmeyer, W., Copeland, R.R. (2000). "Determination of Resistance Due to Shrubs and Woody Vegetation." ERDC/ CHL TR- 00- 25, US Army Corps of Engineers Engineer Research and Development Centre.

Hoerner, S.F. (1965). Fluid-dynamic drag. Bakersfield, California, Hoerner Fluid Dynamics.

Hoffmann, K. (1987). Eine Einführung in die Messung mit Dehnungsmessstreifen. Hrsg. Hottinger und Baldwin Messtrechnik GmbH, Darmstadt Germany.

Järvelä, J. (2006). "Vegetative flow resistance: characterization of woody plants for modeling applications." *World Environmental and Water Resources Congress*, Omaha, USA, papers on CD-Rom.

Keil, S. (1995). Beanspruchungsermittlung mit Dehnungsmessstreifen. Cuneus Verlag. ISBN: 3-9804188-0-4

Lindner, K. (1982). "Der Strömungswiderstand von Pflanzenbeständen." Mitteilungen Leichtweiss-Instituts für Wasserbau, TU Braunschweig, Heft 75.

Statzner, B., Lamoroux, N., Nikora, V., Sagnes, P. (2006). "The debate about drag and reconfiguration of freshwater macrophytes: comparing results obtained by three recently discussed approaches." *Freshwat. Biol.* 51, 2173-2183.

Sumer, B.M., Fredsøe, J. (1997). Hydrodynamics around cylindrical structures. Advanced Series on Ocean Engineering (12).World Scientific, River Edge, N.J.

Vischer, D., Oplatka, M. (1998). "Der Strömungswiderstand eines flexiblen Ufer- und Vorlandbewuchs." *Wasserwirtschaft* 88(6), 284-288.

Vogel, S. (1994). Life in moving fluids: the physical biology of flow. 2nd edition. Princeton, Princeton University Press.

Wilson, C.A.M.E, Hoyt, J., Schnauder, I. (2008). "The impact of foliage on the drag force of vegetation." *ASCE Journal of Hydraulic Engineering*. 134(7), 885-891.

Wilson, C.A.M.E., Schnauder, I., Mas, J., Hoyt, J. (2005). "Measuring the drag force of vegetation." Proc. of the XXI IAHR Congress, Seoul.

Yen, B. C. (2002). "Open channel flow resistance." *ASCE Journal of Hydraulic Engineering.* 128(1), 20-39.